**Electronic supplementary information for:**

# "Hot Edges" in Inverse Opal Structure Enable Efficient $CO_2$ Electrochemical Reduction and Sensitive *in-situ* Raman Characterization

Yang Yang[a,b], Lukas Ohnoutek[c,d], Saira Ajmal[a], Xiuzhen Zheng[a], Yiqing Feng[a], Kejian Li[a], Tao Wang[a], Yue Deng[a], Yangyang Liu[a], Xu Dong[a], Ventsislav K. Valev[c,d]*, Liwu Zhang[a,b]*

[a]*Department of Environmental Science and Engineering, Fudan University; Shanghai, 200433, P. R. China.*

[b]*Shanghai Institute of Pollution Control and Ecological Security, Shanghai, 200092, Peoples' Republic of China*

[c]*Centre for Photonics and Photonic Materials, University of Bath, Bath, BA2 7AY, United Kingdom*

[d]*Centre for Nanoscience and Nanotechnology, University of Bath, Bath, BA2 7AY, United Kingdom*

*E-mail: zhanglw@fudan.edu.cn; v.k.valev@bath.ac.uk*

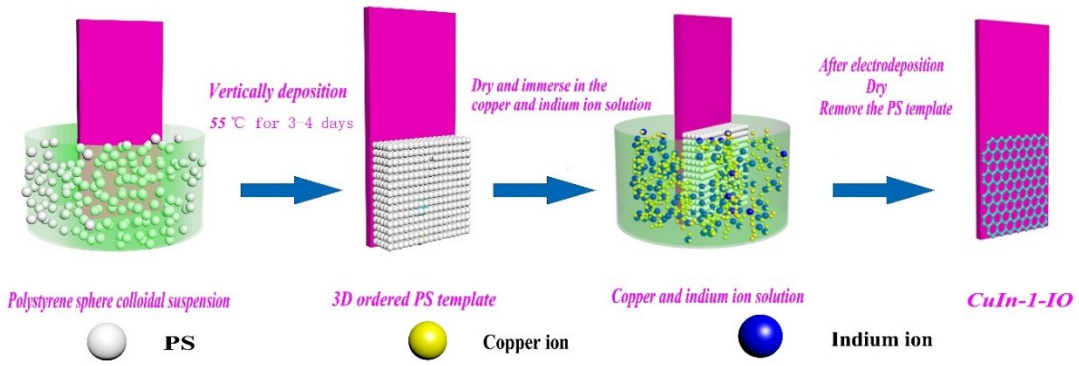


**Scheme S1.** Schematic illustration of the experimental process of fabricating CI-1-IO.

First, the colloidal crystal template of PS beads was formed on fluoride-doped tin oxide (FTO)-covered glass by evaporation-induced self-assembly. Then, the Cu-In alloy was deposited in the void of the template by electro-deposition method. Finally, the obtained Cu-In alloy film was immersed in the tetrahydrofuran (THF) solution to remove the PS template. A planar Cu-In alloy (CI-1) with similar thickness but without the inverse opal structure was also prepared for comparison under identical conditions.

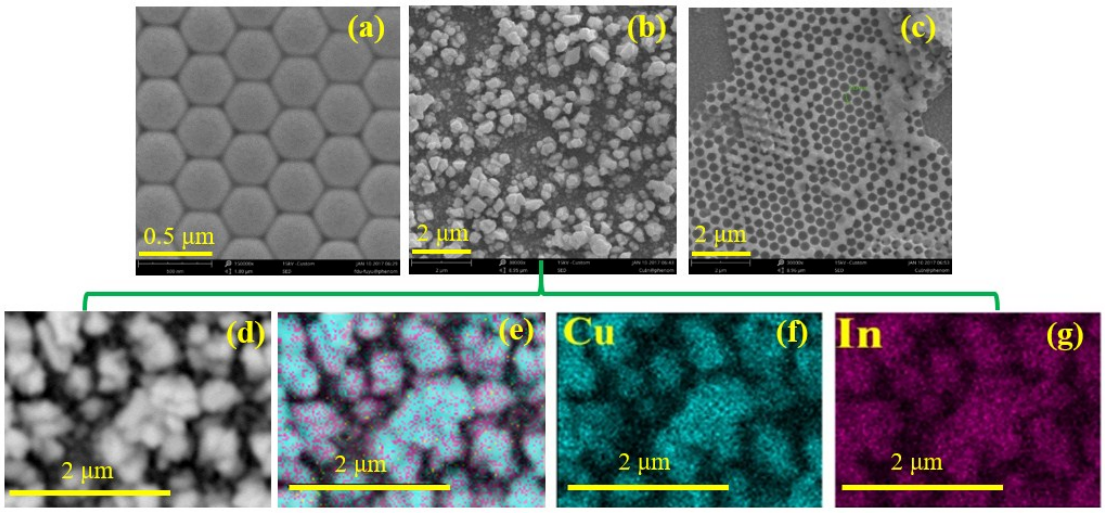


**Fig. S1**. SEM of samples. a) Polystyrenes template. b) CI-1 nanoparticle. c) CI-I-IO. d) Selected area for EDS and e) Element mappings of CI-1 in the rectangular region shown in d. Separated element mappings of f) Cu, g) In in the region shown in e.

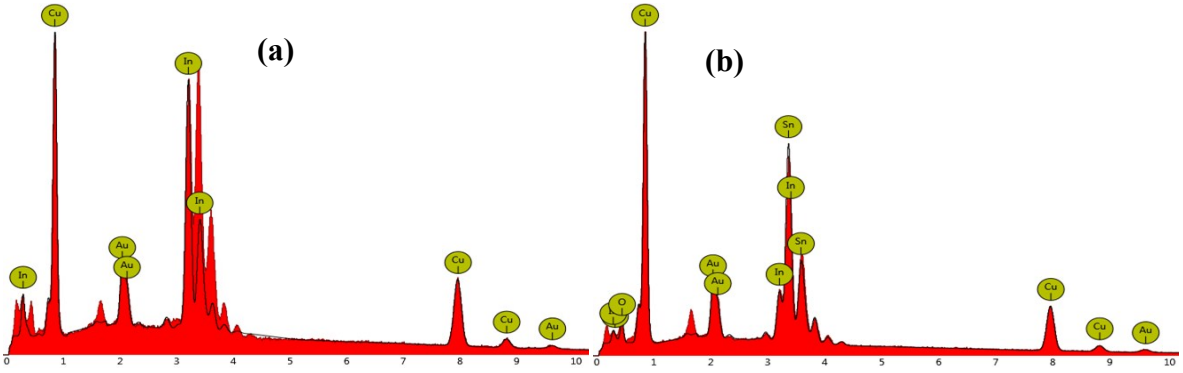


**Fig. S2**. EDX spectra of a) CI-1 and b) CI-1-IO.

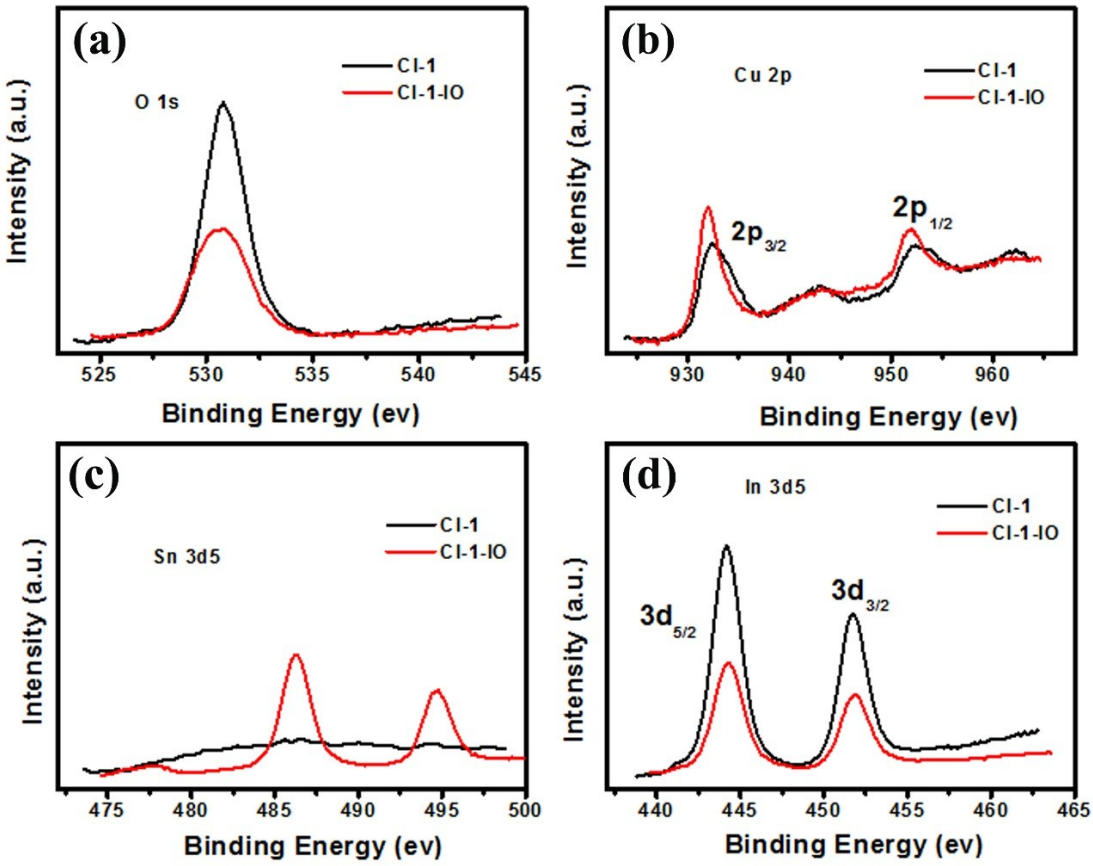


**Fig. S3.** X-ray photoelectron spectra (XPS) spectra of CI-1 and CI-1-IO samples. a) O 1s; b) Cu 2p; c) Sn 3d; d) In 3d.

In order to investigate the chemical states of the samples, X-ray photoelectron spectra (XPS) were studied and are shown in Fig. S3. O 1s spectra are shown in Fig. S3a. The peak around 530 eV can be attributed to the $O^{2-}$ in metal oxides. Fig. S3b shows the Cu 2p spectra. The peaks at approximately 932 and 952 eV correspond to the energy of Cu $2p_{3/2}$ and Cu $2p_{1/2}$ of $Cu_2O$ or Cu.[1] The weak satellite at about 943 eV indicates that a trace amount of $Cu_2O$ has formed on the surfaces of both CI-1 and CI-1-IO. The Sn 3d5 spectra of CI-1 and CI-1-IO are shown in Fig. S3c. The features in the Sn 3d5 spectrum of CI-1-IO are very pronounced. The binding energies around 486 and 495 eV correspond to the Sn (IV) state in $SnO_2$.[2] From Fig. 1a and S1, it can be

seen that for CI-1, the surface of the FTO glass is completely covered by the Cu-In nanoparticles. Therefore, no Sn 3d5 peak is observed for the CI-1 sample. However, for the CI-1-IO sample, a part of the surface of FTO glass is exposed due to the layer having an inverse opal structure. Hence, Sn 3d5 spectra can be detected by XPS on the sample CI-1-IO. In 3d spectra of both CI-1 and CI-1-IO are shown in Fig. S3d, the peaks at about 444 and 452 eV correspond to the In $3d_{5/2}$ and $3d_{3/2}$, indicating the presence of $In^0$ species.[3]

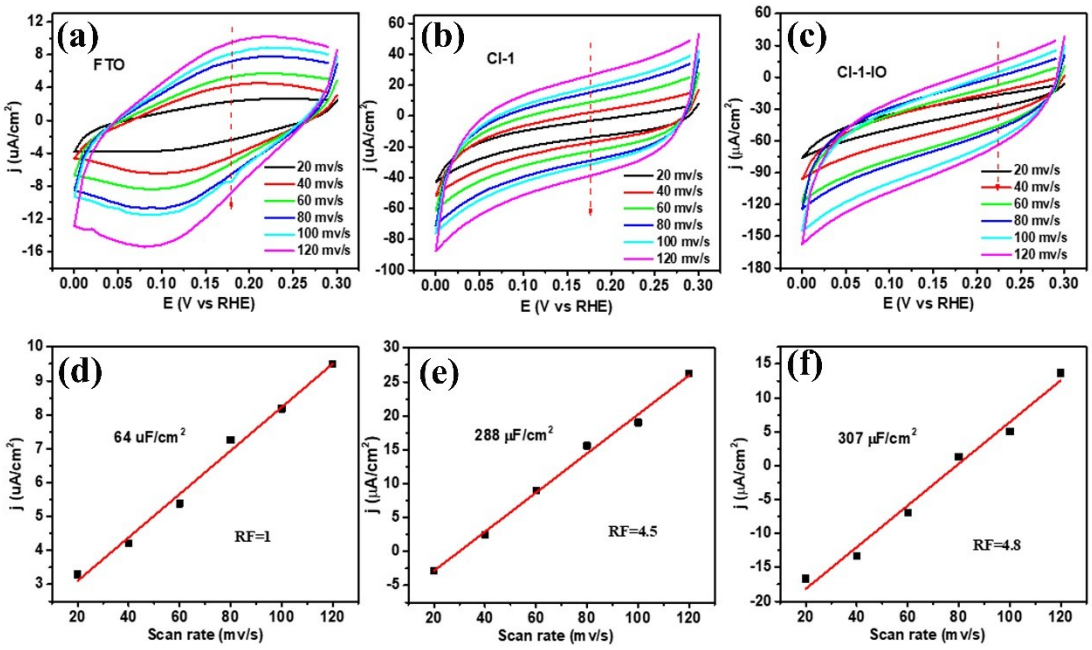


**Fig. S4.** Cyclic voltammetry (CV) curves of a) FTO, b) CI-1 and c) CI-1-IO performed at 0-0.3 V vs RHE range in 0.1 M $KHCO_3$ solution saturated with $N_2$. Corresponded current verse scan rate plots of d) FTO, e) CI-1 and f) CI-1-IO.

The CV curves were taken in 0.1 M $KHCO_3$ electrolyte purged with $N_2$ in the range of 0 to 0.3 V vs RHE, where no Faradic current was obtained. The double layer capacitance was obtained from the slope of the current *vs.* scan rate plot (**Fig. S4**d-f). The RF of the electrodes were calculated from the corresponding capacitance values. The capacitance of FTO is about 64 µF/cm$^2$, which is in accordance with standard capacitance of the smooth oxide metal surface (60 µF/cm$^2$).[4]

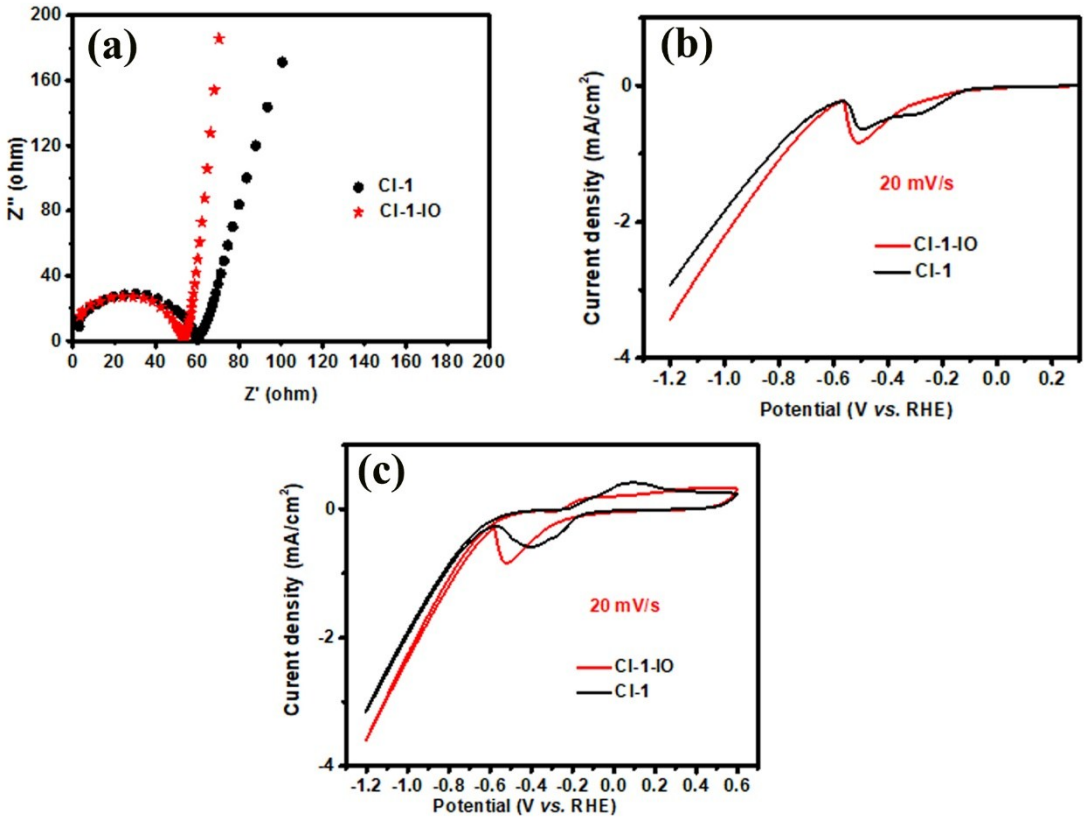


**Fig. S5.** a) Electrochemical impedance spectroscopy (EIS) Nyquist plots of CI-1 and CI-1-IO sample, in the 0.1 Hz – 10 k Hz range, at 0 V *vs.* Ag/AgCl. b) Linear sweep voltammetry (LSV) of CI-1 and CI-1-IO. c) Cyclic voltammetry of CI-1 and CI-1-IO at scanning rate of 20 mv $s^{-1}$. All the characterizations were performed in $CO_2$ saturated 0.1 M $KHCO_3$ solution.

**Fig. S5**b shows the LSV of the samples, it is clearly shown that the current of CI-1-IO is larger than that of CI-1 electrode, which may produce more products. The reduction peak at about 0.59 V *vs.* RHE may be caused by the FTO glass shown in **Fig. S5**c.

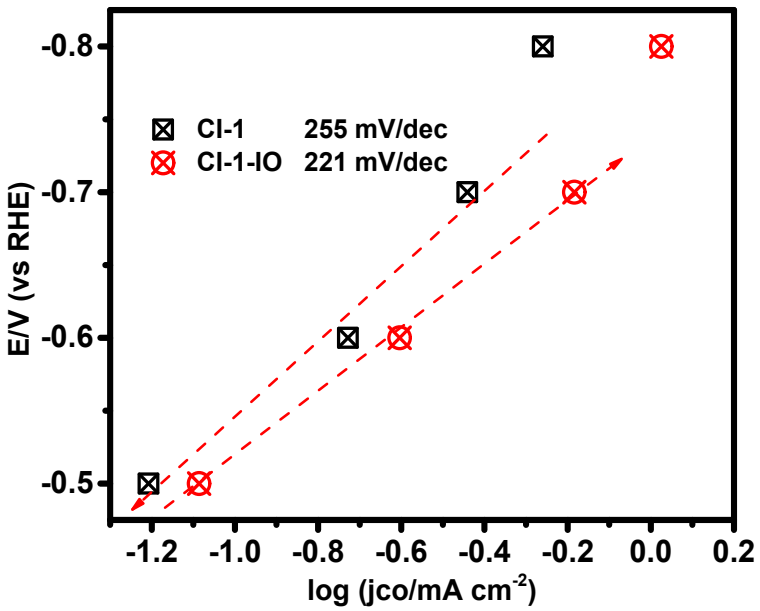


**Fig. S6**. Tafel plot of CI-1 and CI-1-IO.

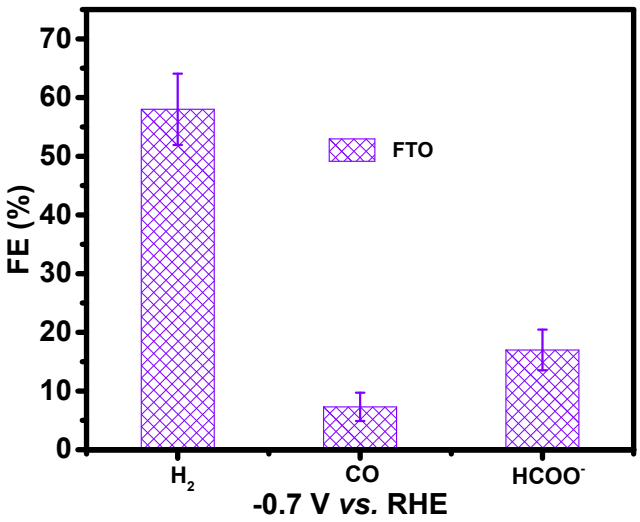


**Fig. S7**. FE of FTO tested in different $KHCO_3$ concentration solutions (saturated with $CO_2$) with external applied potential of -0.7 V *vs.* RHE. The error bar represents the standard deviation of three experiments.

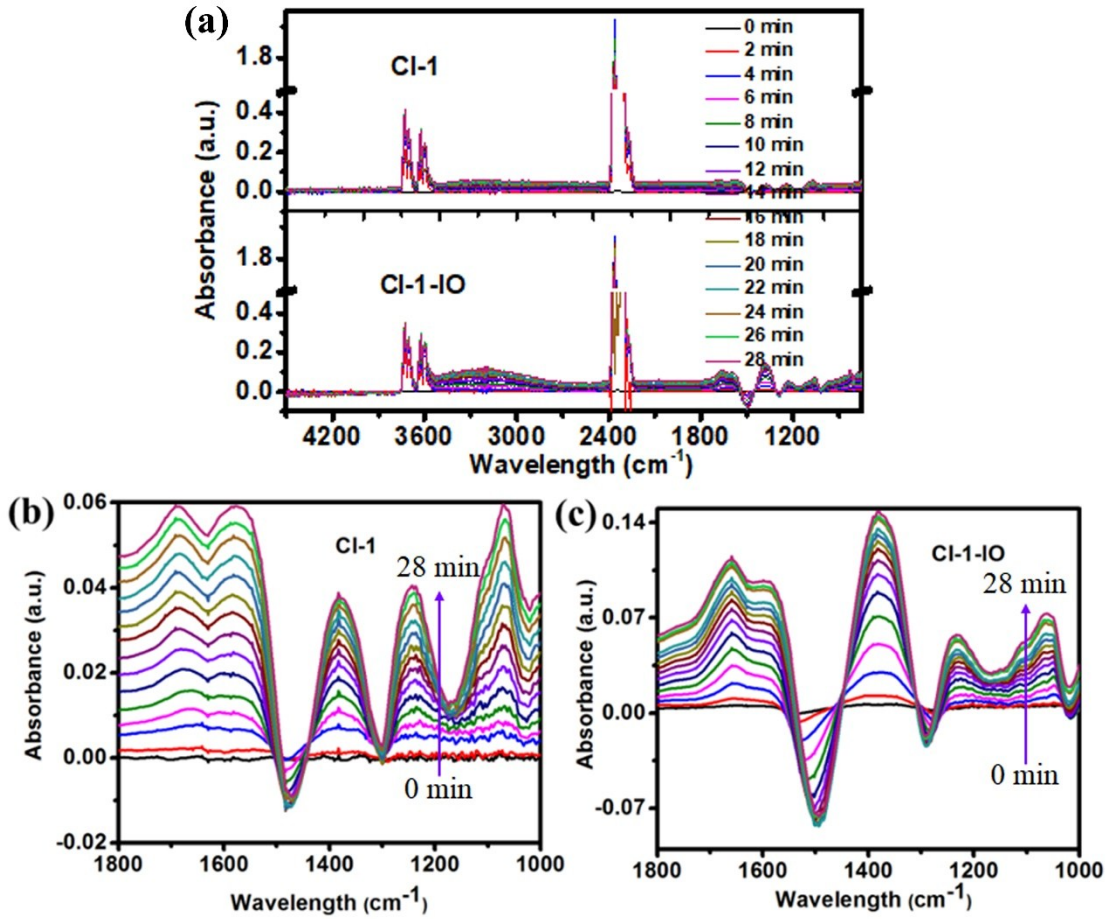


**Fig. S8**. In situ DRIFTS spectra of $CO_2/H_2O$ adsorbed on CI-1 and CI-1-IO surface. (a) Whole spectra from 750-4500, 0-28 min. Spectra regions (1000-1800 $cm^{-1}$) of adsorbed carbonate on b) CI and c) CI-1-IO surface.

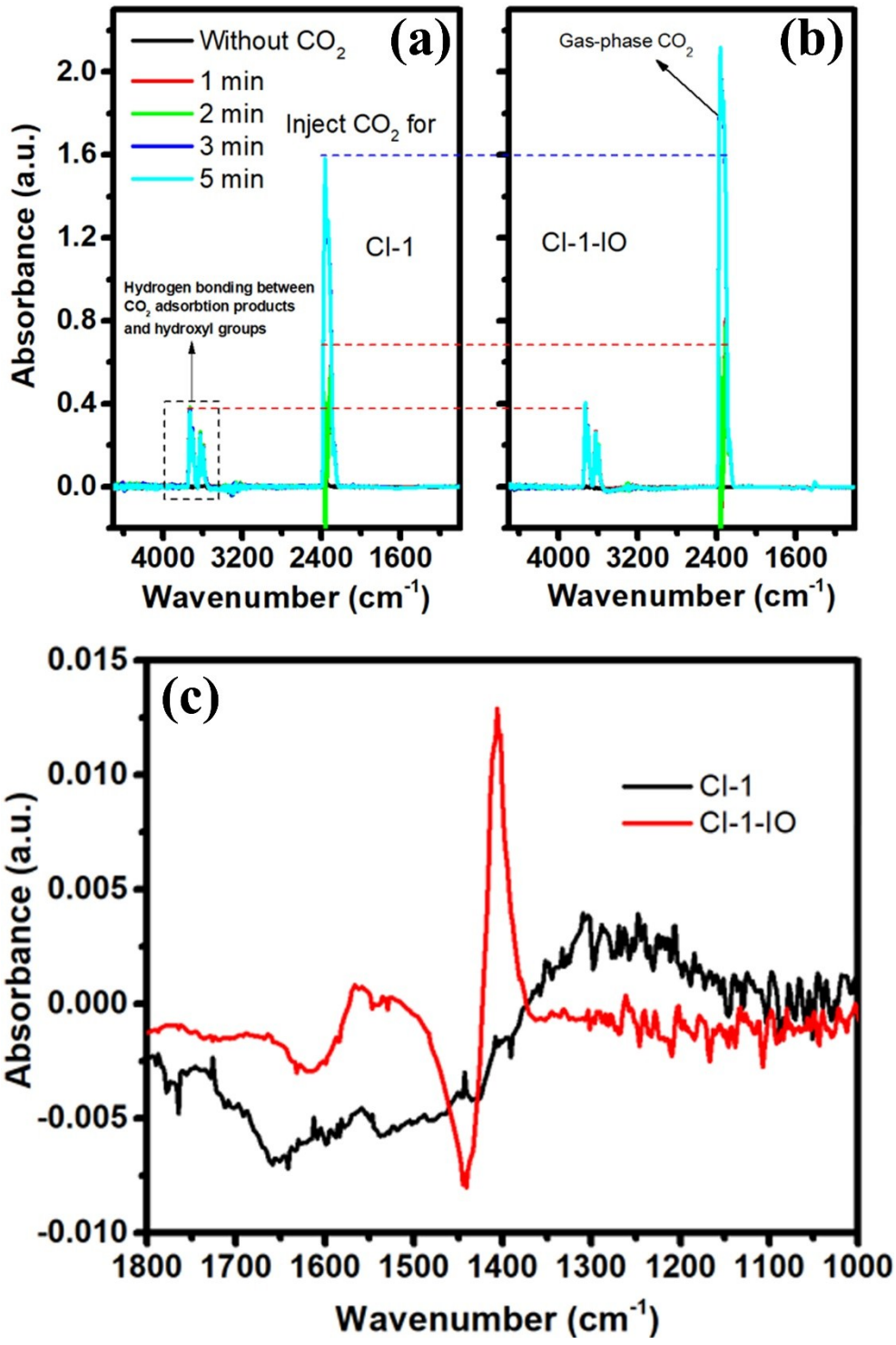


**Fig. S9.** *In-situ* DRIFTS spectra of $CO_2$ adsorbed on the humid a) CI-1 and b) CI-1-IO surface from 0 to 5 min. c) Spectra regions (1000-1800 $cm^{-1}$) of adsorbed carbonate on CI-1 and CI-1-IO surface after 5 min (the spectra are subtracted with its background values).

Firstly, we put the cleaned wet sample into the DRIFTs cell, then vacuumized. After that, the high purity $CO_2$ (99.999%) gas was injected into the cell and the spectra were taken every 1 min. Fig. S9a and b show that the adsorption of $CO_2$ (about 2366 $cm^{-1}$) was saturated for both CI-1 and CI-1-IO in 3 mins. Meanwhile, the CI-1-IO sample shows a higher adsorption capacity of gas-phase $CO_2$ than CI-1. Fig. S9c shows the adsorbed carbonate and bicarbonate at the range of 1000-1800 $cm^{-1}$. The spectra shown in Fig. S9c are obtained from the spectra data of 5 min. It can be seen that the carbonate (1400 $cm^{-1}$) adsorbed on CI-1-IO surface is obviously higher than that of CI-1. The formation of bicarbonate (1200-1300 $cm^{-1}$) on both CI-1 and CI-1-IO are trace, with slightly higher amount on CI-1. These phenomena may be explained by following reasons.

1. As the amount of water on the samples surface are very limited, it will be quickly saturated by the injected $CO_2$ gas, as a result, only a small amount of carbonate and bicarbonate is formed. Because it is wet on the sample surface, it becomes very difficult to obtain the IR signal on the surface ($H_2O$ absorbs IR light strongly).
2. As reported (J. Phys. Chem. C 2007, 111, 14870-14880), at low humidity, the $CO_2$ is likely to react with surface O-H groups to form bicarbonate on the surface; It will react with adsorbed water to yield adsorbed carbonate and surface hydroxyl groups at high humidity. In our case, the relative higher bicarbonate intensity on CI-1 might be caused from the limited surface water.[5]

In summary, these data also support our conclusion that Cu-In alloy with inverse opal structure have a higher capacity for $CO_2$ adsorption.

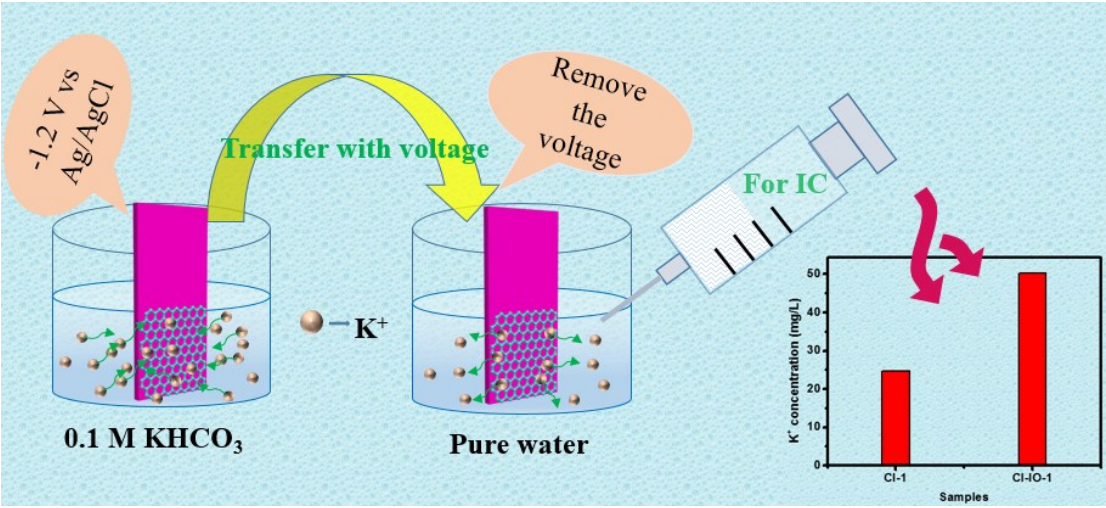


**Fig. S10**. Process of measuring the adsorbed $K^+$ on CI-1 and CI-1-IO. The concentration of $K^+$ released from the electrode surface shown in the insert picture (right side).

First, CI-1 and CI-1-IO electrode were immersed into 0.1 M $KHCO_3$ solution at -1.2 V *vs.* Ag/AgCl for 120 s, and then the electrode was taken out of the solution and immediately put into 10 mL pure water. Then, the applied potential was removed and the adsorbed $K^+$ was thus released into the pure water. Finally, the solution was injected into the IC to check the $K^+$ concentration.

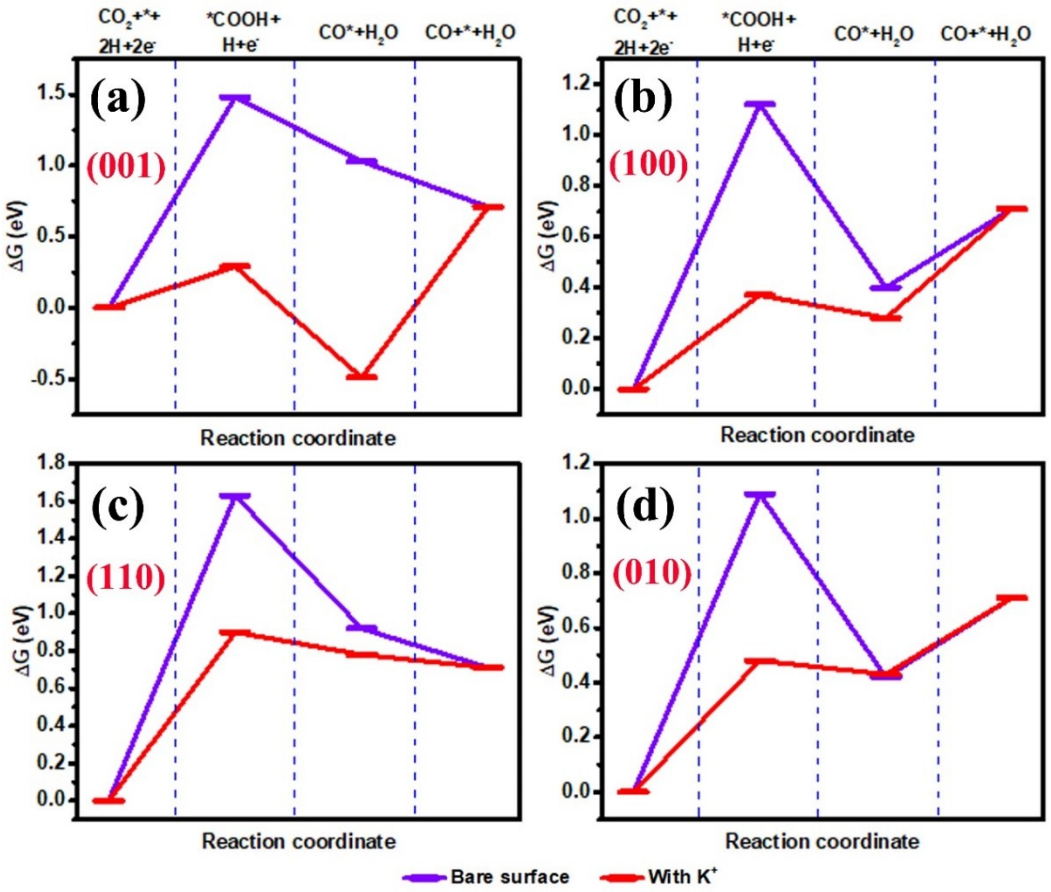


**Fig. S11.** Thermodynamic barriers for $CO_2$ to CO reduction reaction on $Cu_2In$ surface with and without $K^+$. Gibbs free energy of electroreduction of $CO_2$ to CO on $Cu_2In$ a) (001), b) (100), c (110) and d) (010) facets in the presents of adsorbed $K^+$ and without $K^+$.

On $Cu_2In$ (001) facet (**Fig. S11**a), the adsorbed $K^+$ stabilizes the COOH* and CO* intermediates by 1.21 and 1.52 eV, respectively. For $Cu_2In$ (100) and (110) facet, the energy barrier of rate-determining COOH* is lowered by 0.75 and 0.73 eV with the presence of $K^+$, respectively (**Fig. S11**b and c). Meanwhile, **Fig. S11**b and c show that adsorbed $K^+$ stabilizes the CO* by 0.12 and 0.36 eV for the $Cu_2In$ (100) and (110) surface, respectively. On the $Cu_2In$ (010) surface, the adsorbed $K^+$ lowers the energy of COOH* from 1.09 to 0.48 eV, without affecting the CO* intermediates (**Fig. S11**d)

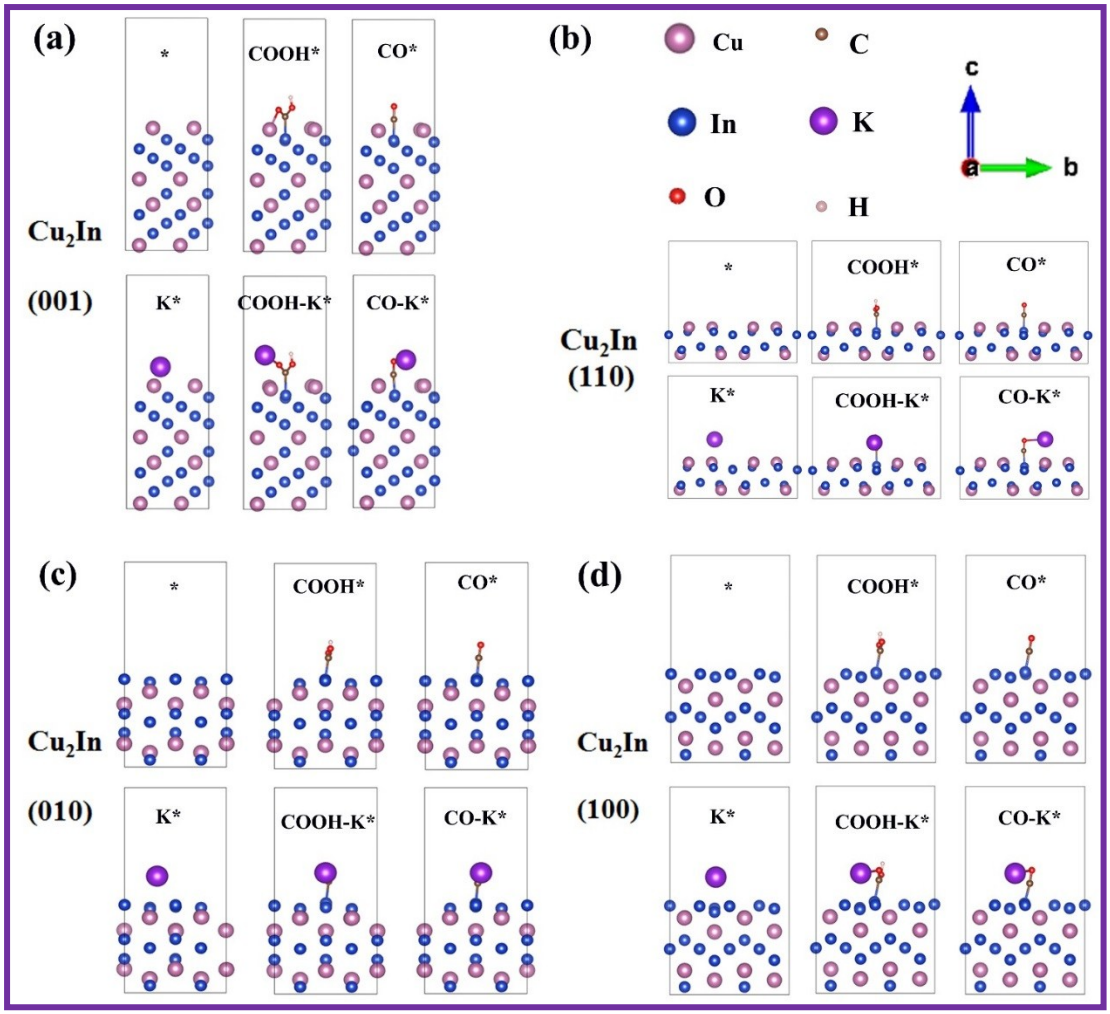


**Fig. S12**. Optimized structure for $Cu_2In$ facets and data calculated with or without $K^+$.

a) $Cu_2In$ (001) facets. b) $Cu_2In$ (110) facets. a) $Cu_2In$ (010) facets. a) $Cu_2In$ (100) facets.

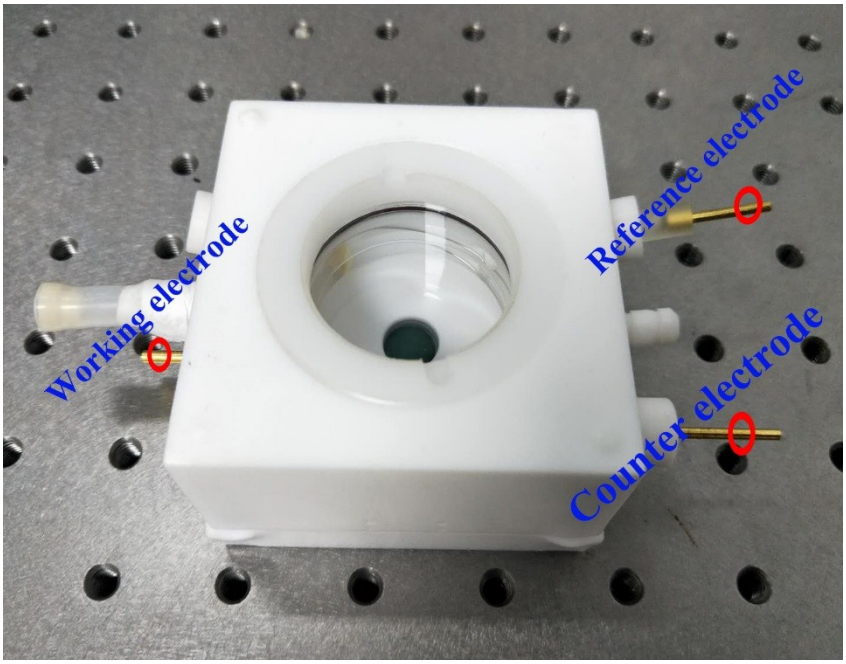


**Fig. S13**. The tailored in situ Raman cell.

**Fig. S13** shows the tailored *in-situ* Raman cell designed by Beijing Scistar Technology Co., Ltd. The distance is about 1 cm form the working electrode surface to the upper quartz window.

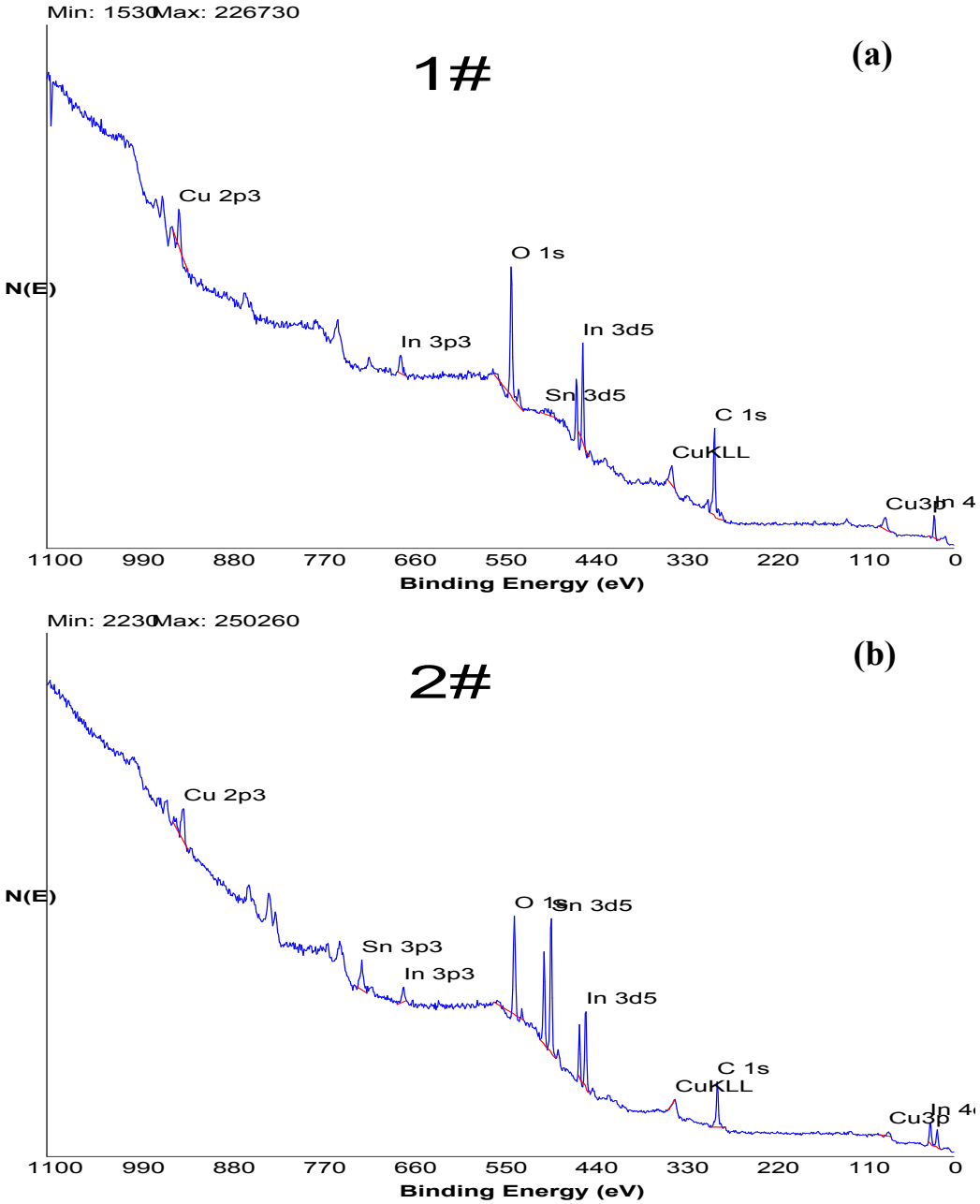


**Fig. S14**. Survey XPS spectra of a) CI-1 and b) CI-1-IO.

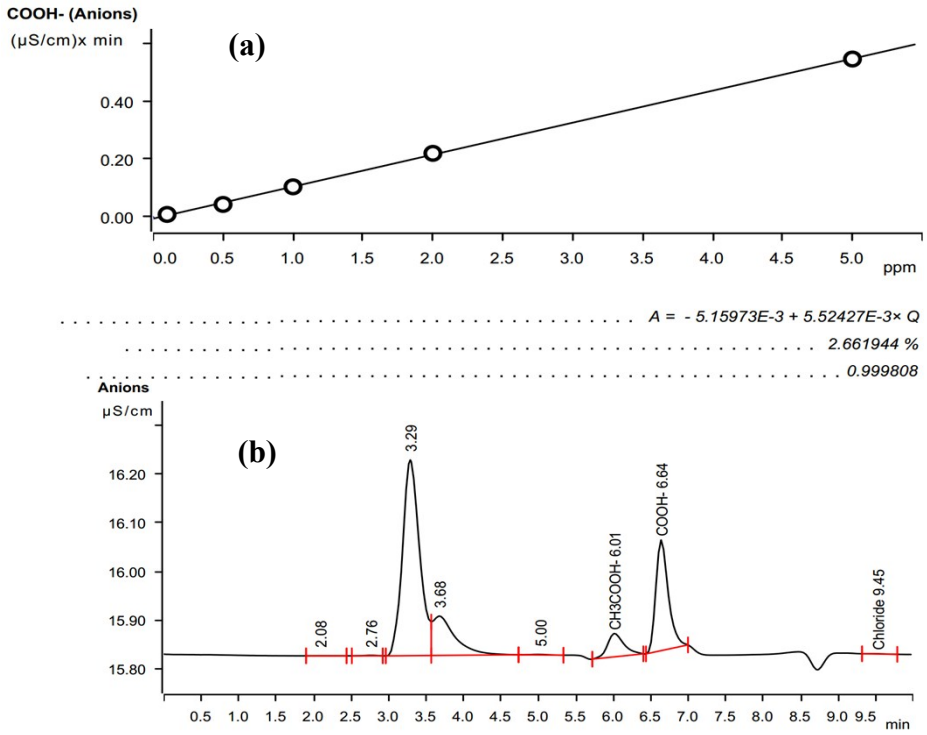


**Fig. S15**. a) Ion chromatography (IC) calibration line of HCOOH standard. b) The IC curve of 0.5 ppm $CH_3COOH$ (6.01 min) and 0.5 ppm HCOOH (6.64 min)

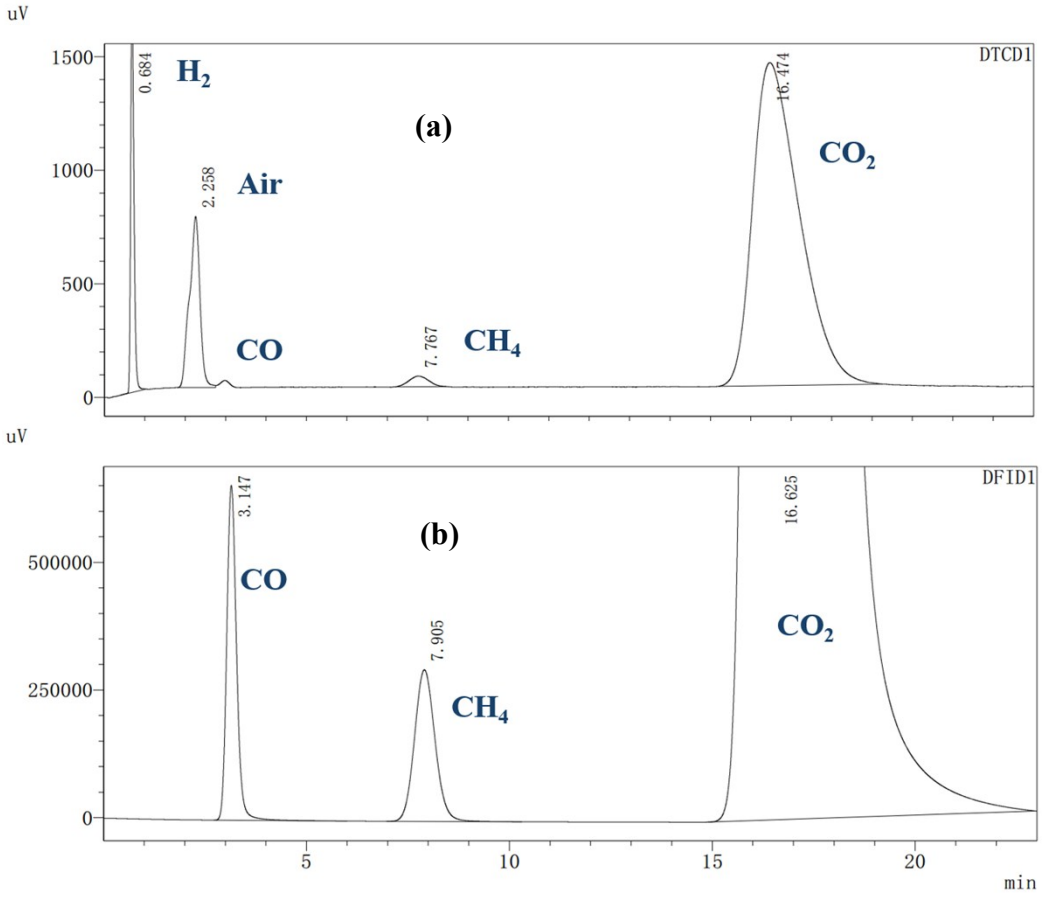


**Fig. S16**. GC curves of standard gas ($H_2$: 245 μmol $L^{-1}$; CO and $CH_4$: 163 μmol $L^{-1}$). a) TCD signal b) FID signal.

**References**


1. X. Q. Qiu, M. Miyauchi, K. Sunada, M. Minoshima, M. Liu, Y. Lu, D. Li, Y. Shimodaira, Y. Hosogi, Y. Kuroda and K. Hashimoto, *ACS Nano*, 2012, **6**, 1609-1618.
2. X. Bai, W. Chen, C. Zhao, S. Li, Y. Song, R. Ge, W. Wei and Y. Sun, *Angew. Chem. Int. Ed. Engl.*, 2017, **56**, 12219-12223.
3. Z. M. Detweiler, J. L. White, S. L. Bernasek and A. B. Bocarsly, *Langmuir*, 2014, **30**, 7593-7600.
4. B. Chi, H. Lin and J. Li, *Int. J. Hydrogen Energy*, 2008, **33**, 4763-4768.
5. J. Baltrusaitis, J. D. Schuttlefield, E. Zeitler, J. H. Jensen and V. H. Grassian, *J. Phys. Chem. C*, 2007, **111**, 14870-14880.